Natural Hazards (2019) 98:575–592
https://doi.org/10.1007/s11069-019-03718-w

ORIGINAL PAPER

Landslides triggered by multiple earthquakes: insights from the 2018 Lombok (Indonesia) events

M. F. Ferrario[1]

Received: 4 March 2019 / Accepted: 2 August 2019 / Published online: 9 August 2019

Abstract
Earthquake-triggered landslides significantly contribute to worsening the impact of seismic events; thus, comprehensive landslide inventories are essential for improving seismic hazard assessment. During complex seismic sequences, landslides are triggered by more than one event and the final inventory reflects the spatial and temporal evolution of the sequence. Here, I analyze the landslides triggered by the 2018 Lombok (Indonesia) seismic sequence. I use high-resolution satellite imagery to map 4823 landslides triggered after the 05/08/2018 event (M_w 6.9) and 9319 landslides after the 19/08/2018 event (M_w 6.9). I analyze the distribution and evolution over time of landslide density and landslide area percentage. Despite the significant increase in number and cumulative area of the landslides, the 05/08 and 19/08 events share the maximum dimension of individual landslides; this suggests that the maximum intensity is equal for the two events, i.e., X on the Environmental Scale Intensity scale. I compare the distribution of landslides with macroseismic information provided by eyewitnesses through online questionnaires. Finally, I investigate the role of earthquake environmental effects within seismic sequences, showing that effects on the natural environment provide complementary information with respect to traditional intensity and felt reports.

Keywords Coseismic landslide · ESI scale · Earthquake environmental effects · Internet macroseismology · Lombok

1 Introduction

Earthquakes and earthquake-induced environmental effects are the deadliest natural phenomena, and since 2000 they caused over 720 thousand fatalities and 530 billion dollars of losses worldwide (CRED 2019). Moderate-to-strong earthquakes are often accompanied by diffuse effects on the environment, such as surface faulting and

Electronic supplementary material The online version of this article (https://doi.org/10.1007/s11069-019-03718-w) contains supplementary material, which is available to authorized users.

✉ M. F. Ferrario
francesca.ferrario@uninsubria.it

[1] Università degli Studi dell'Insubria, via Valleggio 11, Como, Italy

landslides. These impact roads and communication networks, affecting the accessibility and effectiveness of rescue operations during the emergency phase and after the earthquake.

Recent seismic sequences show a high degree of complexity, in terms of spatial and temporal evolution of the earthquakes (e.g., the 2016–2017 Central Italy sequence: Civico et al. 2018), number of ruptured faults (2016 Kaikoura—New Zealand event: Hamling et al. 2017) and distribution of earthquake-triggered effects (2016 Hokkaido—Japan: Yamagishi and Yamazaki 2018; 2018 Palu—Indonesia: Heidarzadeh et al. 2018). These events somehow surprised the scientific community, telling us that our knowledge is still limited. A critical outcome is that the effects of complex sequences, characterized by repeated events in a short time interval (days to months), are not fully addressed in seismic hazard assessment practices.

Landslides are among the most impacting earthquake environmental effects, (EEEs) and the number of earthquakes fatalities is significantly higher if subsequent landslides are triggered (Budimir et al. 2014). Areas impacted by earthquakes become also more prone to landsliding due to subsequent events (earthquakes, rainfall, typhoons, e.g., Lin et al. 2006; Chang et al. 2007). For these reasons, building comprehensive landslide inventories is essential for hazard assessment (Harp et al. 2011). The use of optical and satellite remote-sensed imagery associated with GIS mapping is particularly effective, due to the timely image acquisition which enables the distinction between coseismic features and later movements. Landslide inventories have been compiled for dozens of earthquakes, and global comparisons have been proposed as well (e.g., Keefer 1984; Rodriguez et al. 1999; Malamud et al. 2004; van der Eeckhaut et al. 2007; Harp et al. 2011; Parker et al. 2011; Xu et al. 2013, 2014; Tanyas et al. 2017 and references therein).

Damage produced by earthquakes is assessed through intensity scales, which traditionally are based on the effects on humans, buildings and nature (Wood and Neumann 1931; Musson et al. 2010). Currently, environmental effects are overlooked and intensity is mainly assigned from the effects on man-made structures (e.g., EMS scale, Grünthal 1999). On the contrary, the ESI scale (Environmental Scale Intensity; Michetti et al. 2007; Audemard et al. 2015; Serva et al. 2016; Serva 2019) is based only on EEEs and complements the information provided from traditional, damage-based intensity scales. Beside traditional field surveys, Web-based questionnaires allow to collect a high number of macroseismic data, provided by citizens who felt an earthquake (DYFI "Did You Feel It" approach) and generally expressed in terms of CDI (Community Decimal Intensity; Wald et al. 1999).

Here, I analyze the sequence of $M_w > 6.0$ earthquakes that hit the Lombok (Indonesia) Region in July–August 2018. This paper aims to:

1. Evaluate the number, extent and spatial distribution of earthquake-triggered landslides and assess the maximum intensity through the ESI scale; two inventories are built, related to landslides triggered after the first strong shock and at the end of the seismic sequence.
2. Compare the results of point (1) with the intensity derived from DYFI data.
3. Move toward a generalization, investigating the role of EEEs within complex seismic sequences.

2 Regional setting and the 2018 Lombok seismic sequence

2.1 Seismotectonic setting

Lombok lies in a complex structural setting dominated by the collision between Australian Plate and Sunda Block (Fig. 1), which occurs at a rate up to 70 mm/a. Plate motion is partitioned between megathrust subduction to the S and a 2000-km-long zone of back-arc thrusting to the N (e.g., Koulali et al. 2016). The latter includes the Flores and Wetar Thrusts (Silver et al. 1983; McCaffrey and Nabelek 1987). The Flores Thrust zone encompasses a sequence of imbricated faults running in an E–W direction and marking the transition between subduction of oceanic crust to the W and continental collision to the E (Jones et al. 2014). Slip rates along the Flores Thrust are in the order of 10–20 mm/a, according to GPS measurements (Koulali et al. 2016).

The Flores Thrust was responsible for several strong earthquakes in historical times, including a sequence of events in 1815, 1818 and 1820 (Griffin et al. 2018) and the 1992 Flores event (M_w 7.9; Beckers and Lay 1995), which generated a destructive tsunami. A maximum magnitude of $M_w > 8.0$ is proposed for the Flores Thrust (Nguyen et al. 2015; Griffin et al. 2018), based on the analysis of damage caused by past earthquakes and ground motion modeling.

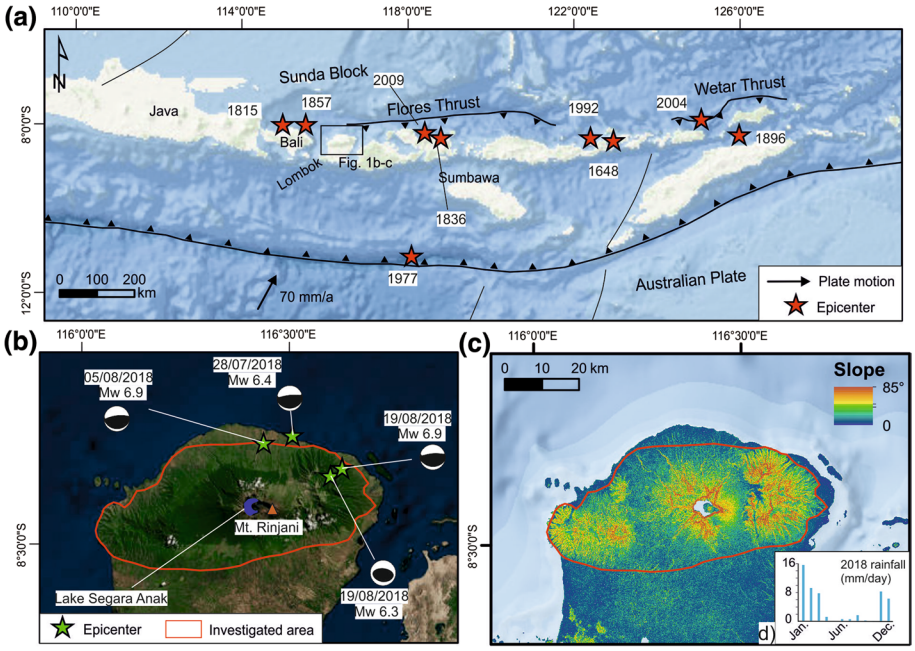

Fig. 1 **a** Seismotectonic setting of the Lombok region: Black arrow shows relative motion between Australian Plate and Sunda Block; topography is from ESRI Ocean Basemap, the black rectangle is the area enlarged in **b** and **c**. **b** Overview of the 2018 seismic sequence. The area where landslides have been mapped is also shown. Focal mechanisms are from USGS. **c** Slope map derived from SRTM elevation model. **d** Monthly rainfall for the year 2018 (PRECL data)

2.2 The study area

The area investigated in the present research lies between latitude 8°15′–8°35′S and longitude 116°0′0″–116°40′0″E (Fig. 1b); it occupies the northern part of Lombok Island for a total of 1798 km^2 and coincides with the region potentially susceptible to landsliding, due to the significant topographic relief (Fig. 1c). The area is dominated by the Rinjani Volcanic Complex, comprising Mt. Rinjani (3726 m asl) and the Samaras caldera presently occupied by Lake Segara Anak and resulting from a Plinian eruption occurred in 1257 (Lavigne et al. 2013). The investigated area lies entirely on volcanic rocks, including tuffs, lavas, volcanic and pyroclastic deposits of Mt. Rinjani (Mangga et al. 1994). The average slope is 16°; highest values occur on the shores of Lake Segara Anak and in the eastern part of the investigated area.

Lombok is highly susceptible to landsliding due to the rugged mountainous terrain, the presence of weathered volcanic sediments and the humid tropical climate (Cepeda et al. 2010). Temperatures are almost constant throughout the year (27–33 °C); precipitation concentrates between November and March, whereas the dry season is between April and October (see Fig. 1d for 2018 rainfall data). The inner part of the island is covered by dense vegetation and hosts spare population; on the contrary, the flat coastal region shows a high degree of vulnerability due to the significant population and infrastructures.

2.3 The 2018 earthquakes

In July–August 2018, the Lombok region was hit by four $M_w > 6.0$ earthquakes in less than one month (Fig. 1b, Table 1). The seismic sequence started on 28/07/2018 with a M_w 6.4 event with epicenter located inland; on 05/08/2018, a M_w 6.9 event occurred 8 km to the SW and on 19/08/2018, two events (M_w 6.3 and M_w 6.9) struck 15 km to the SE of the first shock. All the events present a thrust mechanism and nucleated at a depth of 14–34 km along the Flores Thrust zone.

Permanent ground deformation revealed by Insar analysis reaches up to 40 cm of line-of-sight displacement after the 05/08 event (GSI, 2018). According to Shakemap models (USGS 2018), ground motion reached 0.4 g and 0.7 g in the 05/08 and 19/08 events, respectively. A small tsunami with waves up to 50 cm was observed after the 05/08 event. The sequence caused 588 fatalities (CRED 2019) and widespread damage.

Table 1 Summary of the $M_w > 6.0$ events occurred during the 2018 Lombok seismic sequence. Data from USGS

Date	Hour	Latitude	Longitude	M_w	Depth
28/07/2018	22:47:38	−8.24	116.508	6.4	14
05/08/2018	11:46:38	−8.258	116.438	6.9	34
19/08/2018	04:10:22	−8.337	116.599	6.3	16
19/08/2018	14:56:27	−8.319	116.627	6.9	21

3 Materials and methods

3.1 Landslide inventories

Landslides were digitized on a GIS platform based on computer screen-based visual interpretation of high-resolution aerial images. Sentinel-2 data (10 m resolution) were used to obtain a regional overview of triggered landslides, whereas mapping was realized over PlanetScope (3 m resolution) imagery. Ortho-rectified 4-band multispectral tiles were used (Planet Team 2017), selecting those with low cloud coverage. Few meters of misalignment between satellite images were observed; this issue is negligible for the scope of the present paper, because it does not affect landslide number or area.

Landslide identification was based on the analysis of contrast in color and texture between pre-event imagery and post-event imagery; shallow landslides are clearly recognizable on aerial imagery because they stripped off the vegetation, resulting in denuded regions. For realizing the inventory of landslides triggered by the 05/08 event, I used PlanetScope images acquired on 08/08/2018. This inventory follows the M_w 6.4 event of 28/07/2018 and the M_w 6.9 event of 05/08/2018; a complete mapping of failures induced by the 28/07 event was not possible due to persistent cloud cover; however, no significant landslides are recognized in the cloud-free portions of available imagery for the 01/08/2018 event. Thus, the mapped landslides are largely the result of the M_w 6.9 event of 05/08/2018, as already pointed out by Ganas et al. (2018). Preexisting landslides were recognized from images taken in July 2018 (before the first shock); these were included in the inventory only if they were reactivated by the sequence.

For the inventory of the 19/08 event, I used images acquired between 20/08/2018 and 27/09/2018. Since post-earthquakes' images are taken within 1 month following the sequence and in the dry season (August and September precipitation: 1.75 and 0.28 mm/day; Fig. 1d), very few non-seismic landslides are expected.

Following the guidelines proposed in the literature (Malamud et al. 2004; Harp et al. 2011), all individual landslides were represented as polygons and mapped as long as they can be recognized from images. To avoid biases related to amalgamation (Marc and Hovius 2015), multiple polygons were drawn when small failures coalesce into a larger landslide.

In order to analyze the spatial characteristics of landslide distribution, two descriptors were adopted: landslide density and landslide area percentage (LAP). First, a grid of 1 km × 1 km squares was created; then, landslide density was computed as the number of individual landslides per unit area; landslide centroids were used for data computation. LAP is the percentage of the area covered by the landslide polygons.

Landslide polygons are provided as supplementary material in kmz format.

3.2 Macroseismic intensity assessment

Seismological information and maps of expected ground motion (shakemaps) and ground failures (landslides and liquefaction) were retrieved from the USGS Web site. Intensity reported by eyewitnesses through the compilation of online questionnaires (DYFI—"Did You Feel It" approach, Wald et al. 1999) was downloaded as aggregated intensities in geocoded boxes using UTM coordinate boundaries of 1 km size. Data are expressed in CDI scale (Community Decimal Intensity).

The spatial distribution of landslides and DYFI data was then compared to the population density determined from the Landscan database of global population distribution. Landscan represents an ambient population (average over 24 h) distribution with a spatial resolution of about 1 km^2 (30″ × 30″).

4 Results

4.1 Distribution of earthquake-triggered landslides

The 05/08 inventory comprises 4823 landslides, whereas after the 19/08 events, 9319 landslides are mapped throughout the investigated area; the majority of mapped landslides is of the shallow disrupted type. Landslides concentrate on steep slopes, and the most affected area lies along a NW–SE-oriented region W of Mt. Rinjani (Fig. 2). Very few landslides are located in the coastal region, mainly along river channels (Ganas et al. 2018; Fig. 2f).

Following Malamud et al. (2004), a landslide magnitude scale is defined as the logarithm to the base 10 of the total number of landslides (N_{LT}) associated with the event:

$$m_L = \log_{10}\left(N_{LT}\right)$$

The resulting landslide magnitudes for the 05/08 and 19/08 events are 3.68 and 3.96, respectively.

Summing up the areas of individual landslides, a total of 4.88 and 10.25 km^2 (i.e., 0.3–0.6% of the investigated area) is obtained for the 05/08 and 19/08 events. The average area of individual landslides is 1012 and 1100 m^2, respectively.

The most significant landslide in terms of area is a complex slope movement 3 km SE of Mt. Rinjani, occupying 150,000 m^2 (i.e., 1.4% of the total landslide area; Fig. 2d). The average concentration is 2.7 and 5.2 landslides/km^2. Maximum values are 76 and 84 landslides/km^2 for the 05/08 and 19/08 inventories.

Figure 3 presents the thematic maps of landslide density and landslide area percentage (LAP) for the 05/08 and 19/08 inventories. The LAP matches well with landslide density, showing high values (up to 15.3 and 20.3% for the 05/08 and 19/08 inventories) in the same region. A general trend of increasing LAP with increasing landslide density is observed (R^2 0.4; Fig. 3c); obvious outliers are individual very wide landslides (low-density, high LAP, e.g., Fig. 2d) and numerous small movements aligned along watercourses (high-density, low LAP, e.g., Fig. 2f).

The landslide inventories realized in the present study can be compared with the outputs of the ground failure model developed by USGS, which provides near-real-time estimates of earthquake-triggered landslide and liquefaction hazard following significant earthquakes worldwide (Nowicki Jessee et al. 2018). The USGS model seems to underpredict the actual effects, because significant landslide hazard (estimated area exposed to hazard: 25 km^2) is expected for the 05/08/2018 event, but limited hazard (estimated area < 2 km^2) is expected for the 19/08 events. The spatial distribution of expected landslides differs from the actual distribution, because the highest hazard is expected on the shores of Lake Segara Anak and in the NE part of Lombok Island; on the contrary, the region most extensively impacted lies where low hazard is expected. These discrepancies highlight the need of further increasing the performance of ground failure models (Tanyas et al. 2017).

Starting from the two inventories, I compute an area–frequency distribution, according to the equation (Malamud et al. 2004):

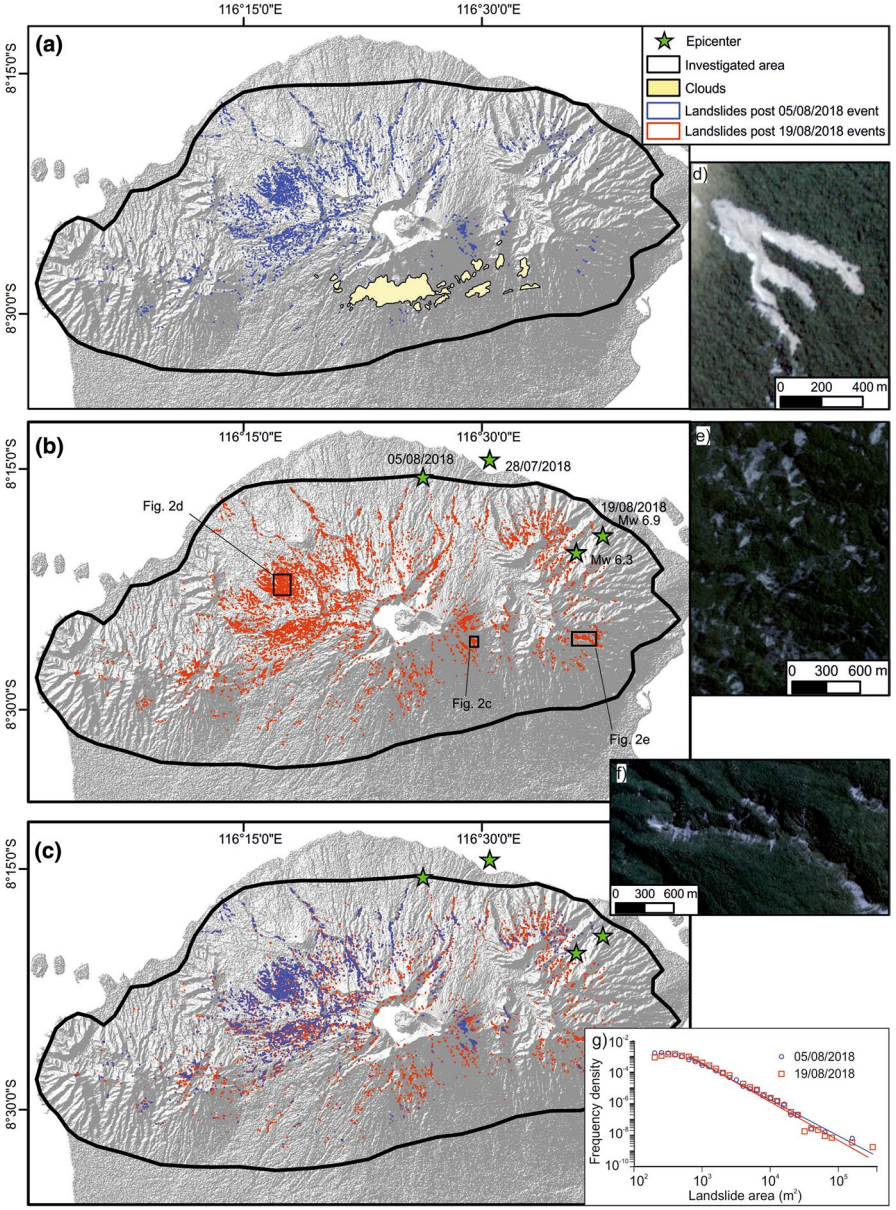

Fig. 2 **a** Inventory map of landslides triggered after the 05/08/2018 event; **b** inventory map of landslides triggered after the 19/08/2018 event; **c** inventory of the 05/08 event superimposed on the inventory of the 19/08 events; **d–f** examples of triggered landslides (PlanetScope imagery taken on 09/09/2018, position shown in **b**); **g** frequency–magnitude curve for the 05/08 and 19/08 inventories

$$p = \frac{1}{N}\frac{\delta N_{\mathrm{L}}}{\delta A_{\mathrm{L}}}$$

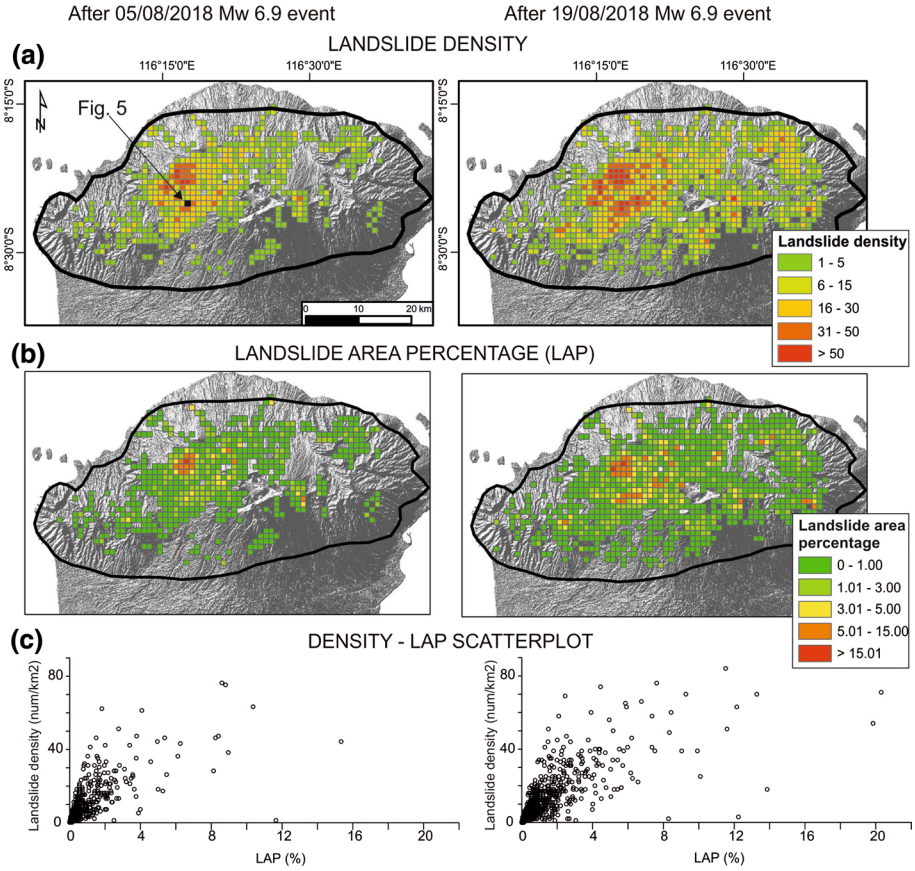

Fig. 3 **a** Landslide density of the 05/08/2018 (left) and 19/08/2018 (right) events; **b** landslide area percentage; **c** scatter plots of landslide density versus landslide area percentage

where N is the total number of landslides in the inventory and δN_L is the number of landslides with area between A_L and $A_L + \delta A_L$; a log-linear increase between A_L and $A_L + \delta A_L$ is adopted, so that bin width is equal in logarithmic coordinates. Size frequency distribution typically exhibits a negative power-law scaling for moderate to large landslides and a positive power-law scaling for small landslides, separated by a rollover representing the modal average of the dataset. This fact has been documented for several case histories (e.g., Malamud et al. 2004; van der Eeckhaut et al. 2007; Xu et al. 2014; Massey et al. 2018; Roback et al. 2018; Valagussa et al. 2019).

For the Lombok case (Fig. 2g), the rollover corresponds to 200–400 m^2. For values above the rollover, the exponent of the power-law scaling (i.e., slope of the area–frequency curve) is -2.29 and -2.41 for the 05/08 and 19/08 inventories, respectively. These values agree with those reported for other inventories worldwide (exponent of -2.3 ± 0.6; van der Eeckhaut et al. 2007), suggesting a near complete landslide inventory.

Given the number of landslides triggered by an earthquake, Malamud et al. (2004) proposed equations to estimate the total landslide area and largest landslide area. Considering the 4823 and 9319 landslides triggered by the 05/08 and 19/08 events, a total

landslide area of 14.72–28.41 km^2 and the largest landslide area of 0.47–0.75 km^2 are expected. Observed values are slightly lower than predicted ones (total area 4.87–10.39 km^2; largest individual landslide 0.15 km^2), possibly due to the limited area prone to landsliding or inherent variability in landslide occurrence in different events.

4.2 "Did You Feel It" data

Figure 4 presents the distribution of intensity data derived from online questionnaires and collected as average intensities on a 1-km^2 grid. Data are expressed as Community Decimal Intensity which, contrary to other macroseismic scales, results in decimal rather than ordinal values of assigned intensities. When compared to the area investigated for landslide occurrence, DYFI data cover a much larger region, with reports up to 1800 km far from the epicenter. For the 28/07 and 19/08 events, over 75% of the data belong to intensity lower than 5, whereas for the 05/08 event this percentage decreases to 37% (Fig. 4d). Highest values reach CDI intensity of 8.6, 9.1 and 7.3 for the 28/07, 05/08 and 19/08 events, respectively.

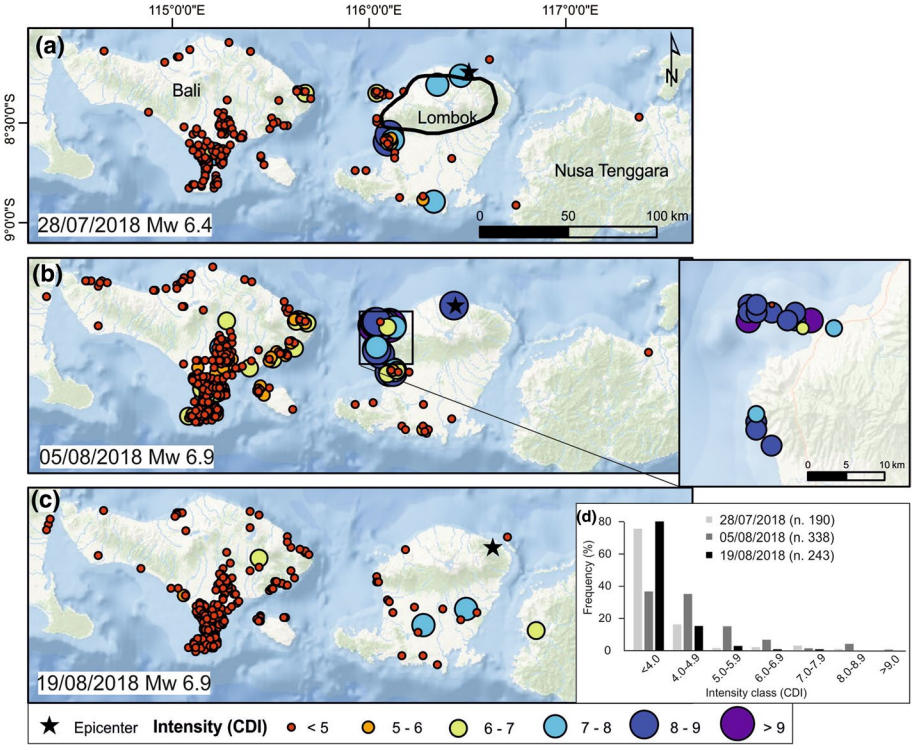

Fig. 4 Community Decimal Intensity derived from DYFI data: **a** 28/07/0218; **b** 05/08/2018 and zoom on West Lombok; **c** 19/08/2018; **d** frequency of observations in terms of intensity classes

5 Discussion

5.1 Evolution through time: the cumulative effect

The occurrence of multiple earthquakes in a short time interval inherently affects the assessment of earthquake effects and their areal distribution. This fact has significant consequences (1) when earthquakes within a seismic sequence are quite distant, enlarging the affected areas and (2) for pre-instrumental seismic sequences, where source parameters are directly derived from earthquake effect, lacking instrumental observations.

In Fig. 5a, I show an example of the evolution in time of the landslides triggered by the Lombok seismic sequence for a 1-km^2-wide region: the pre-event imagery, taken on 02/07/2018, shows no sign of preexisting landslides; after the 05/08 event (i.e., imagery taken on 08/08/2018), several slope movements can be recognized; finally, in the imagery taken on 13/09/2018, the number and dimensions of landslides are sensibly increased.

The progression of landslide density and LAP between the two inventories is shown in Fig. 5b, c, respectively. Each point represents the value of a single 1 km^2 cell used for density and LAP computation; if no changes occurred between the 05/08 and 19/08 inventories, the points are aligned along the 1:1 line. The graphs show indeed a noticeable increase: The 19/08 inventory contains a number of individual landslides twice than the 05/08 inventory, resulting in higher density and LAP.

In this study, I quantitatively compared landslide inventories obtained during and at the end of a seismic sequence; this approach can be successfully exported elsewhere for studying the cumulative effect of repeated earthquakes. The possibility to accurately map individual landslides and their evolution over time is a trade-off between data availability

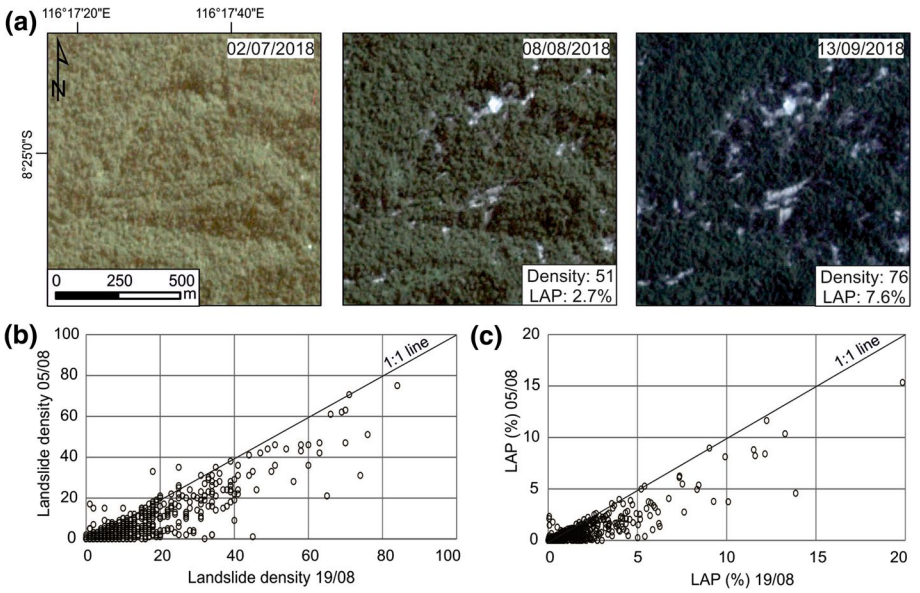

Fig. 5 **a** Example of the evolution of landslide occurrence before, during and after the seismic sequence (PlanetScope imagery), see Fig. 3 for location; **b** Landslide density changes between the 05/08 and 19/08 inventories; **c** LAP changes between the 05/08 and 19/08 inventories

and the evolution of the seismic sequence. Satellite imagery should be acquired as soon as possible after the earthquake, but persistent cloud cover and satellite revisiting time can be limiting factors. Field surveys can be difficult due to terrain ruggedness and damage on road networks and infrastructures.

5.2 Intensity assessment: ESI scale and comparison with Community Decimal Intensity

I used landslide density and LAP to define the maximum intensity, according to the ESI scale guidelines (Table 2; Michetti et al. 2007, Serva et al. 2016). Hancox et al. (2002) developed criteria for assessing macroseismic intensity (MM—Modified Mercalli scale) from landslide distribution of historical earthquakes in New Zealand. More recently, Xu et al. (2013) quantified thresholds for intensity assessment in terms of landslide concentration and LAP for the 2008 Wenchuan earthquake. Here, I do not provide quantitative thresholds due to: (1) the slightly different information given by landslide density and LAP (Fig. 3c), (2) the difficulty in comparing various macroseismic scales (e.g., Xu et al. 2013 is based on the Chinese intensity scale) and (3) the fact that for intensity higher than X, ESI intensity is based on the total area affected by landslides, rather than the dimension of individual landslides or their total number (Table 2).

The definition of the ESI intensity class is based mainly on two criteria: (Table 2): (1) dimension of individual landslides in terms of volume and (2) total dimension of the area affected by landslides. For the Lombok case history, the latter criterion cannot be applied because offshore regions prevent the possibility to obtain a complete macroseismic field. This problem is commonly encountered in coastal regions, either using damage-based CDI or ESI scales.

In the present study, the evaluation of maximum ESI intensity is based on the dimension of the biggest landslide (Fig. 2d): This has a 150,000 m^2 area and was triggered by the 05/08 event. No bigger landslides result from the 19/08 event; thus, I assign a maximum ESI intensity of X to both the 05/08 and 19/08 events. This value is higher than CDI intensity either for the 05/08 and 19/08 events. For intensities higher than X, traditional scales tend to saturate, and thus, environmental effects represent the better way to assess macroseismic intensity (Michetti et al. 2007; Papanikolaou and Melaki 2017). Previous studies also found that in the epicentral region, ESI is higher than damage-based intensity (Sanchez and Maldonado 2016; Chunga et al. 2018). Beside saturation phenomena, it must be recalled that CDI values are aggregated intensities rather than individual datapoints, possibly affecting the maximum values.

Another result worth mentioning is that the CDI values of the 19/08 event are lower than that of 05/08 event and that very few reports derive from West Lombok (Fig. 4c). Despite differences in seismological parameters (e.g., wave path, directivity) cannot be ruled out, a plausible explanation is that the 19/08 event struck a region already severely damaged by the previous events, and thus, people evacuated the area when the seismic swarm started and/or are unable or not willing to contribute their response to the USGS website.

Figure 6a shows the population density of Lombok Island and nearby regions. The southern part and the entire coastal area of Lombok are densely inhabited (thousands of people per km^2), whereas the mountainous northern half of the island has a very low population density. When analyzed according to population density, DYFI data and mapped landslides are clearly complementary (Fig. 6b, c): Of the over 700 DYFI data used in the present study, one single point lies in the area investigated for landslide occurrence. More

Table 2 Classification of ESI 2007 intensity based on landslide distribution and affected area (after Serva et al. 2016)

ESI Intensity	Landslides occurrence	Landslide volume (m^3)	Affected area (km^2)
V	Rare failures on steep slopes		
VI	Frequent failures on steep slopes	10	< 1
VII	Scattered landslides occur in prone areas	10^3–10^5	< 10
VIII	Small to moderate landslides widespread in prone areas	10^5–10^6	< 100
IX	Landsliding widespread in prone areas, also on gentle slopes; their size is frequently large, sometimes very large	10^5–10^6	< 1000
X	Large landslides and rockfalls are frequent, practically regardless of equilibrium state of the slopes.	10^5–10^6	< 5000
XI	Large landslides and rockfalls are frequent, practically regardless of equilibrium state of the slopes. Significant landslides can occur at 200–300 km distance from the epicenter	> 10^6	< 10,000
XII	Large landslides and rockfalls are frequent, practically regardless of equilibrium state of the slopes. Significant landslides can occur at 200–300 km distance from the epicenter	> 10^6	50,000

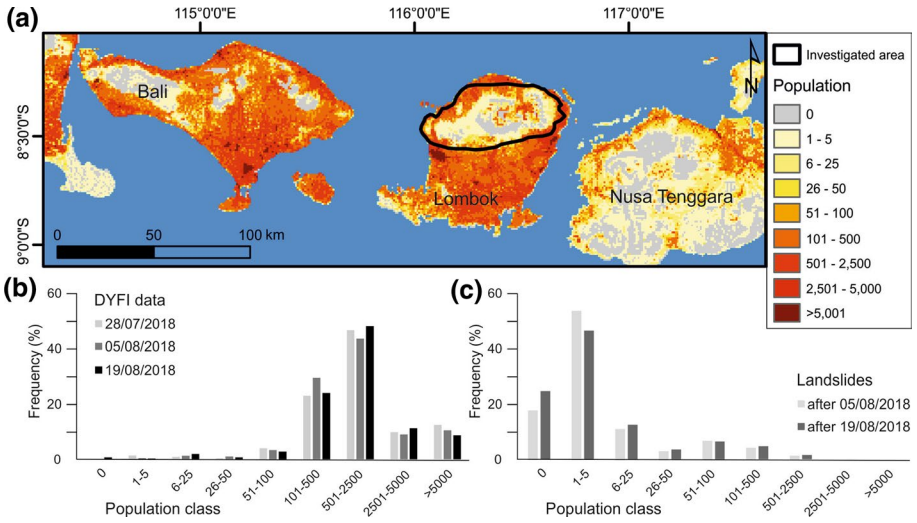

Fig. 6 **a** Population density of the study area (Landscan database); **b** frequency of DYFI data according to population classes; **c** frequency of landslides according to population classes

than 90% of DYFI data correspond to population density higher than 100 people/km^2, whereas more than 90% of mapped landslides lie in region with less than 100 people/km^2.

5.3 Moving toward a generalization: the role of environmental effects within seismic sequences

Complex seismic sequences pose a relevant challenge in terms of risk evaluation and mitigation, because the impact at the end of the sequence can be much worse than after the mainshock. The current practice in seismic risk assessment is not tailored to deal with complex seismic sequences, given the Poissonian assumption and earthquake catalog declustering (Guidoboni and Valensise 2015).

For instance, the 19/08 events struck an area already hit by previous shocks, which changed the vulnerability of the physical and the built environments. The progression of damage is closely related to the spatial and temporal evolution of the seismic sequence. If a built structure is already damaged by an earthquake and then hit by a subsequent event, it is not possible to isolate the damage associated with the last event; damage assessed at the end of the sequence thus reflects the cumulative effect (Rossi et al. 2019).

Similarly, if a landslide is reactivated after each shock, it is possible to retrieve the cumulative landslide dimension; to ascertain the contribution of each shock is problematic, because one should evaluate to which extent vulnerability has changed after the former shocks. Nevertheless, the spatial distribution of landslides triggered by each event offers useful insights. The upper bound of expected landslide occurrence as a function of magnitude (Keefer 1984) can be related to the area affected by EEEs as defined in the ESI scale (Table 2). In Fig. 7, I use the 2018 Lombok and 2015 Gorkha (Nepal) seismic sequences as case histories.

Let us discuss the Lombok case at first. For a M_w 6.9 event, landslides are expected in a ca. 12,000-km^2-wide region, which corresponds to the boundary between intensity

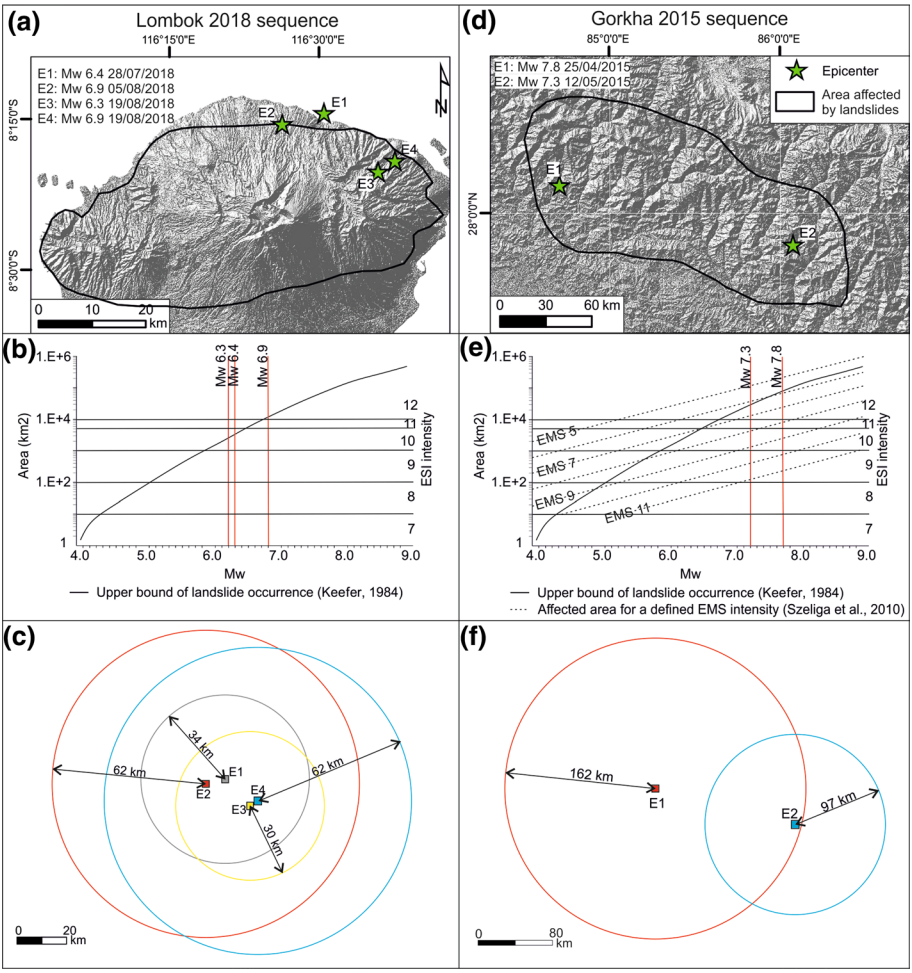

Fig. 7 **a** 2018 Lombok epicenters; **b** expected areas of landslide occurrence as a function of moment magnitude (left axis; Keefer 1984) and comparison with ESI intensity degrees (right axis); **c** schematic sketch of the regions where landslides are expected, given the epicenter location shown in **a**; **d–f** same as a–c applied to the 2015 Gorkha (Nepal) sequence

XI and XII on the ESI scale. For M_w 6.3–6.4, the area affected by landslides is up to 2800–3600 km^2, i.e., ESI IX. In Fig. 7c, I draw circles around the epicenters of the Lombok events, with radius equivalent to the expected maximum distance obtained from Keefer's relations, assuming azimuthal symmetry (i.e., a circular area). The circles largely overlap due to the closeness of the epicenters, and the total affected area is slightly larger than the area expected from a single M_w 6.9 event.

In Fig. 7d–f, I apply the same approach to the 2015 Gorkha seismic sequence. A M_w 7.8 event occurred on 25/04/2015 along the Main Himalayan Thrust, followed by several aftershocks, including a M_w 7.3 on 12/05/2015, located 140 km to the E–SE (Martha et al. 2017; Roback et al. 2018). The sequence caused more than 15,000 landslides, which were mapped from high-resolution satellite data. Landslides triggered by the mainshock and the M_w 7.3 aftershock were separately identified (Martha et al. 2017).

For the Gorkha case study, the area affected by landslides can be compared also with the areas where a certain intensity is expected. Szeliga et al. (2010) developed an intensity attenuation relation, where intensity (expressed as EMS-98—European Macroseismic Scale, Grünthal 1999) is calculated as a function of moment magnitude M_w and hypocentral distance R according to the following equation:

$$I = a + bM_w + cR + d\log R$$

For the Himalayan Region, $a = 6.05 \pm 0.94$, $b = 1.11 \pm 0.10$, $c = -0.0006 \pm 0.0006$ and $d = -3.91 \pm 0.38$. Solving the equation for M_w, magnitude can be calculated for each intensity class for a set of hypocentral distances. Assuming a circular area of macroseismic fields, I compute the areas encompassed by each isoseismal; the results are plotted in Fig. 7e.

For a M_w 7.8 event, landslides are expected in a 83,000 km^2 wide area (up to 160 km from the epicenter), and for a M_w 7.3 in a 29,500 km^2 wide area (up to 96 km from the epicenter), which correspond to the area encompassed by the isoseismal VI on the EMS-98 scale (Fig. 7e; Szeliga et al. 2010). From Fig. 7f, it is evident that the cumulative area where landslides are expected extends 100 km to the E than the one assumed for the strongest shock.

6 Conclusions

The conclusions arising from the present study can be summarized as follows:

- I compiled two landslide inventories, pertaining to the 05/08 and 19/08/2018 events that hit the Lombok region; they include 4823 and 9319 polygons, with a total area of 4.87 and 10.39 km^2, respectively. I compute landslide density and landslide area percentage on a 1-km^2 grid, and I analyze the evolution over time as well.
- I assessed the maximum ESI intensity as X for the two events. The spatial distribution of earthquake-induced landslides is complementary to felt reports gathered by USGS through the DYFI approach.
- I evaluate the role of earthquake-triggered landslides as a tool to investigate the cumulative pattern of damage caused by complex seismic sequences.
- Earthquake environmental effects and the ESI scale can flank information deriving from effects on humans and the built environment, allowing to comprehensively capture the complexity of seismic sequences, particularly in remote areas. In this sense, the timely acquisition of integrated datasets and the realization of comprehensive inventories of environmental effects will ultimately improve seismic risk assessment and mitigation.

Acknowledgements I want to thank Franz Livio and Alessandro Michetti for fruitful discussion and the two anonymous reviewers; Planet for providing PlanetScope imagery as part of the Education and Research program and ESA for Copernicus Sentinel data. Did You Feel It data are retrieved from the USGS website (https://earthquake.usgs.gov/data/dyfi/). PRECL Precipitation data provided by the NOAA/OAR/ESRL PSD, Boulder, Colorado, USA, from their Web site at https://www.esrl.noaa.gov/psd/. Aster GDem is a product of METI and NASA. LandScan 2017™ High Resolution global Population Data Set is copyrighted by UT-Battelle, LLC, operator of Oak Ridge National Laboratory under Contract No. DE-AC05-00OR22725 with the United States Department of Energy.

Compliance with ethical standards

Conflict of interest The authors declare that they have no conflict of interest.

References

Audemard FA, Azuma T, Baiocco F, Baize S, Blumetti AM, Brustia E, Clague J, Comerci V, Esposito E, Guerrieri L, Gürpinar A, Grützner C, Jin K, Kim YS, Kopsachilis V, Lucarini M, McCalpin J, Michetti AM, Mohammadioun B, Mörner N A, Okumura K, Ota Y, Papathanassiou I, Pavlides S, Pérez-López R, Porfido S, Reicherter K, Rodríguez-Pascua MA, Rogozhin E, Scaramella A, Serva L, Silva P, Sintubin M, Tatevossian R, Vittori E (2015) Earthquake environmental effect for seismic hazard assessment: the ESI intensity scale and the EEE Catalogue. Memorie Descrittive della Carta Geologica d'Italia, vol 97. ISPRA, Servizio Geologico D'Italia

Beckers J, Lay T (1995) Very broadband seismic analysis of the 1992 Flores, Indonesia, earthquake ($M_w = 7.9$). J Geophys Res 100(B9):18179–18193. https://doi.org/10.1029/95jb01689

Budimir MEA, Atkinson PM, Lewis HG (2014) Earthquake-and-landslide events are associated with more fatalities than earthquakes alone. Nat Hazards 72:895–914. https://doi.org/10.1007/s11069-014-1044-4

Cepeda J, Smebye H, Vangelsten B, Nadim F, Muslim D (2010) Landslide risk in Indonesia. Global assessment report on disaster risk reduction, ISDR. https://www.preventionweb.net/english/hyogo/gar/2011/en/bgdocs/Cepeda_et_al._2010.pdf Accessed Jan 2019

Chang KT, Chiang SH, Hsu ML (2007) Modeling typhoon- and earthquake-induced landslides in a mountainous watershed using logistic regression. Geomorphology 89(2007):335–347

Chunga K, Livio F, Mulas M, Ochoa-Cornejo F, Besenzon D, Ferrario MF, Michetti AM (2018) Earthquake ground effects and intensity of the 16 April 2016 M_w 7.8 Pedernales, Ecuador, Earthquake: implications for the source characterization of large subduction earthquakes. Bull Seismol Soc Am. https://doi.org/10.1785/0120180051

Civico R, Pucci S, Villani F, Pizzimenti L, De Martini PM, Nappi R, Open EMERGEO Working Group (2018) Surface ruptures following the 30 October 2016 M_w 6.5 Norcia earthquake, central Italy. J Maps 14(2):151–160

CRED—Centre for Research on the Epidemiology of Disasters (2019). https://www.emdat.be/. Accessed Jan 2019

Ganas A, Tsironi V, Valkaniotis S (2018) A preliminary report on the 2018 Lombok region Indonesia earthquakes. https://www.emsc-csem.org/Files/news/Earthquakes_reports/Lombok%20earthquake%20report%20GTV%209-8-2018.pdf. Accessed Jan 2019

Griffin J, Nguyen N, Cummins P, Cipta A (2018) Historical earthquakes of the Eastern Sunda Arc: source mechanisms and intensity-based testing of Indonesia's National Seismic Hazard Assessment. Bull Seismol Soc Am. https://doi.org/10.1785/0120180085

Grünthal G (ed) (1999) European Macroseismic Scale 1998 (EMS-98), Cahiers du Centre Européen de Géodynamique et de Séismologie, vol 15. Centre Européen de Géodynamique et de Séismologie, Luxembourg, p 99

GSI (Geospatial Information Authority of Japan) (2018) The 2018 Lombok Island, Indonesia Earthquake: crustal deformation detected by ALOS-2 data, update 30 August 2018. http://www.gsi.go.jp/cais/topic180731-index-e.html. Accessed Jan 2019

Guidoboni E, Valensise G (2015) On the complexity of earthquake sequences: a historical seismology perspective based on the L'Aquila seismicity (Abruzzo, Central Italy), 1315–1915. Earthq Struct 8:153–184

Hamling IJ, Hreinsdóttir S, Clark K, Elliott J, Liang C, Fielding E et al (2017) Complex multifault rupture during the 2016 M_w 7.8 Kaikōura earthquake, New Zealand. Science 356(6334):eaam7194

Hancox GT, Perrin ND, Dellow GD (2002) Recent studies of historical earthquake-induced landsliding, ground damage, and MM intensity in New Zealand. Bull N Z Soc Earthq Eng 35(2):59–95

Harp EL, Keefer DK, Sato HP, Yagi H (2011) Landslide inventories: the essential part of seismic landslide hazard analyses. Eng Geol 122(1–2):9–21

Heidarzadeh M, Muhari A, Wijanarto AB (2018) Insights on the source of the 28 September 2018 Sulawesi Tsunami, Indonesia based on spectral analyses and numerical simulations. Pure Appl Geophys. https://doi.org/10.1007/s00024-018-2065-9

Jones ES, Hayes GP, Bernardino M, Dannemann FK, Furlong KP, Benz HM, Villaseñor A (2014) Seismicity of the Earth 1900–2012 Java and vicinity: U.S. Geological Survey Open-File Report 2010–1083-N, 1 sheet, scale 1:5,000,000. https://dx.doi.org/10.3133/ofr20101083N

Keefer DK (1984) Landslides caused by earthquakes. Geol Soc Am Bull 95(4):406–421
Koulali A, Susilo S, McClusky S, Meilano I, Cummins P, Tregoning P, Lister G, Efendi J, Syafi'i MA (2016) Crustal strain partitioning and the associated earthquake hazard in the eastern Sunda-Banda Arc. Geophys Res Lett 43:1943–1949. https://doi.org/10.1002/2016GL067941
Lavigne F, Degeai JP, Komorowski JC, Guillet S, Robert V, Lahitte P, Oppenheimer C, Stoffel M, Vidal CM, Surono Pratomo I, Wassmer P, Hajdas I, Hadmoko DS, de Belizal E (2013) Source of the great A.D. 1257 mystery eruption unveiled, Samalas volcano, Rinjani Volcanic Complex, Indonesia. PNAS 110:16742–16747. https://doi.org/10.1073/pnas.1307520110
Lin CW, Liu SH, Lee SY, Liu CC (2006) Impacts of the Chi-Chi earthquake on subsequent rainfall-induced landslides in central Taiwan. Eng Geol 86(2006):87–101
Malamud BD, Turcotte DL, Guzzetti F, Reichenbach P (2004) Landslide inventories and their statistical properties. Earth Surf Process Landf 29:687–711. https://doi.org/10.1002/esp.1064
Mangga S, Atmawinata S, Hermanto B, Setyogroho B (1994) Geological Map of The Lombok Sheet, West Nusa Tenggara, scale 1:250.000. Geological Research and Development Centre, Bandung
Marc O, Hovius N (2015) Amalgamation in landslide maps: effects and automatic detection. Nat Hazards Earth Syst Sci 15:723–733. https://doi.org/10.5194/nhess-15-723-2015
Martha TR, Roy P, Mazumdar R, Govindharaj KB, Kumar KV (2017) Spatial characteristics of landslides triggered by the 2015 M_w 7.8 (Gorkha) and M_w 7.3 (Dolakha) earthquakes in Nepal. Landslides 14(2):697–704
Massey C, Townsend D, Rathje E, Allstadt KE, Lukovic B, Kaneko Y, Bradley B, Wartman J, Jibson RW, Petley DN, Horspool N, Hamling I, Carey J, Cox S, Davidson J, Dellow S, Godt JW, Holden C, Jones K, Kaiser A, Little M, Lyndsell B, McColl S, Morgenstern R, Rengers FK, Rhoades D, Rosser B, Strong D, Singeisen C, Villeneuve M (2018) Landslides Triggered by the 14 November 2016 M_w 7.8 Kaikoura Earthquake, New Zealand. Bull Seismol Soc Am. https://doi.org/10.1785/0120170305
McCaffrey R, Nabelek J (1987) Earthquakes, gravity, and the origin of the Bali basin: an example of a nascent continental fold-and-thrust belt. J Geophys Res 92(B1):441–460
Michetti AM, Esposito E, Guerrieri, Porfido S, Serva L, Tatevossian R, Vittori E, Audemard F, Azuma T, Clague J et al (2007) Environmental Seismic Intensity Scale 2007—ESI 2007, Memorie Descrittive della Carta Geologica d'Italia, vol 74, Servizio Geologico d'Italia, Dipartimento Difesa del Suolo, APAT, Rome, Italy, 7–54. http://www.isprambiente.gov.it/en/publications/technical-periodicals/descriptive-memories-of-the-geological-map-of/intensity-scale-esi-2007?set_language=en. Accessed Dec 2018
Musson RMW, Grünthal G, Stucchi M (2010) The comparison of macroseismic intensity scales. J Seismol 14(2):413–428
Nguyen N, Griffin J, Cipta A, Cummins PR (2015) Indonesia's historical earthquakes: modelled examples for improving the national hazard map, Geoscience Australia Record 2015/23, Canberra, Australia
Nowicki Jessee MA, Hamburger MW, Allstadt K, Wald DJ, Robeson SM, Tanyas H, Hearne M, Thompson EM (2018) A global empirical model for near-real-time assessment of seismically induced landslides. J Geophys Res Earth Surf 123:1835–1859. https://doi.org/10.1029/2017JF004494
Papanikolaou I, Melaki M (2017) The Environmental Seismic Intensity Scale (ESI 2007) in Greece, addition of new events and its relationship with magnitude in Greece and the Mediterranean; preliminary attenuation relationships. Quat Int 451:37–55
Parker RN, Densmore AL, Rosser NJ, de Michele M, Li Y, Huang RQ, Whadcoat S, Petley DN (2011) Mass wasting triggered by 2008 Wenchuan earthquake is greater than orogenic growth. Nat Geosci 4(7):449–452
Planet Team (2017) Planet application program interface: in space for life on earth. San Francisco, CA. https://api.planet.com
Roback K, Clark MK, West AJ, Zekkos D, Lin G, Gallen SF, Chamlagain D, Godt JW (2018) The size, distribution, and mobility of landslides caused by the 2015 Mw7.8 Gorkha earthquake, Nepal. Geomorphology 301:121–138
Rodriguez C, Bommer JJ, Chandler RJ (1999) Earthquake-induced landslides: 1980–1997. Soil Dyn Earthq Eng 18(1999):325–346
Rossi A, Tertulliani A, Azzaro R, Graziani L, Rovida A, Maramai A, Pessina V, Hailemikael S, Buffarini G, Bernardini F, Camassi R, Del Mese S, Ercolani E, Fodarella A, Locati M, Martini G, Paciello A, Paolini S, Arcoraci L, Castellano C, Verrubbi V, Stucchi M (2019) The 2016–2017 earthquake sequence in Central Italy: macroseismic survey and damage scenario through the EMS-98 intensity assessment. Bull Earthq Eng. https://doi.org/10.1007/s10518-019-00556-w
Sanchez JJ, Maldonado RF (2016) Application of the ESI 2007 scale to two large earthquakes: South Island, New Zealand (2010 M_w 7.1), and Tohoku, Japan (2011 M_w 9.0). Bull Seismol Soc Am 106(3):1151–1161

Serva L (2019) History of the Environmental Seismic Intensity Scale ESI-07. Geosciences 9:210. https://doi.org/10.3390/geosciences9050210

Serva L, Vittori E, Comerci V, Esposito E, Guerrieri L, Michetti AM, Mohammadioun B, Mohammadioun GC, Porfido S, Tatevossian RE (2016) Earthquake hazard and the Environmental Seismic Intensity (ESI) scale. Pure Appl Geophys 173(5):1479–1515. https://doi.org/10.1007/s00024-015-1177-8

Silver EA, Reed D, McCaffrey R, Joyodiwiryo Y (1983) Back-arc thrusting in the Eastern Sunda Arc Indonesia: a consequence of arc-continent collision. J Geophys Res 88(B9):7429–7448. https://doi.org/10.1029/JB088iB09p07429

Szeliga W, Hough S, Martin S, Bilham R (2010) Intensity, magnitude, location, and attenuation in India for felt earthquakes since 1762. Bull Seismol Soc Am 100(2):570–584. https://doi.org/10.1785/012008032 9

Tanyaş H, van Westen CJ, Allstadt KE, Anna Nowicki Jessee M, Görüm T, Jibson RW, Sato HP, Schmitt RG, Marc O, Hovius N (2017) Presentation and analysis of a worldwide database of earthquake-induced landslide inventories. J Geophys Res Earth Surf 122:1991–2015. https://doi.org/10.1002/2017JF004236

USGS (2018) https://earthquake.usgs.gov/earthquakes/eventpage/us1000gda5/executive#executive. Accessed Jan 2019

Valagussa A, Marc O, Frattini P, Crosta GB (2019) Seismic and geological controls on earthquake-induced landslide size. Earth Planet Sci Lett 506(2019):268–281

van der Eeckhaut M, Poesen J, Govers G, Verstraeten G, Demoulin A (2007) Characteristics of the size distribution of recent and historical landslides in a populated hilly region. Earth Planet Sci Lett 256(2007):588–603

Wald DJ, Quitoriano V, Dengler L, Dewey JW (1999) Utilization of the internet for rapid community intensity maps. Seismol Res Lett 70(6):680–697

Wood HO, Neumann F (1931) Modified Mercalli intensity scale of 1931. Bull Seismol Soc Am 21:277–283

Xu C, Xu X, Zhou B, Yu G (2013) Revisions of the M 8.0 Wenchuan earthquake seismic intensity map based on co-seismic landslide abundance. Nat Hazards 69:1459–1476. https://doi.org/10.1007/s11069-013-0757-0

Xu C, Shyu JBH, Xu X (2014) Landslides triggered by the 12 January 2010 Port-au-Prince, Haiti, $M_w = 7.0$ earthquake: visual interpretation, inventory compiling, and spatial distribution statistical analysis. Nat Hazards Earth Syst Sci 14:1789–1818. https://doi.org/10.5194/nhess-14-1789-2014

Yamagishi H, Yamazaki F (2018) Landslides by the 2018 Hokkaido Iburi-Tobu Earthquake on September 6. Landslides. https://doi.org/10.1007/s10346-018-1092-z